Phytoplankton bloom in the Gulf of Elat/Aqaba: physical vs. ecological forcing

Hadar Berman[1] and Hezi Gildor[2]

[1]The Hebrew University of Jerusalem
[2]The Hebrew University

November 24, 2022

Abstract

Phytoplankton bloom in the Gulf of Elat/Aqaba was studied before mainly using one-dimensional models and observations from the northern Gulf. Thus, the spatial variability within the Gulf and the contribution of physical processes such as horizontal advection to the bloom have not yet been studied. Moreover, various factors such as light limitation are still debated. Here we used a three-dimensional coupled physical-ecological model for the Gulf of Elat/Aqaba to study the mechanisms for phytoplankton bloom throughout the Gulf. We found the southern surface bloom to be higher than the northern surface. In contrast, southern integrated bloom is lower than the northern bloom. These differences are due to spatial variations in the mixed layer depth, which
is much deeper in the northern Gulf compared with the south. Moreover, horizontal advection controls phytoplankton integrated biomass during the bloom, a process often neglected when dealing with phytoplankton
blooms. Finally, we found that light limits growth of the northern integrated bloom.

Phytoplankton bloom in the Gulf of Elat/Aqaba: physical vs. ecological forcing

Hadar Berman[1], **Hezi Gildor**[1]

[1]The Institute of Earth Sciences, The Hebrew University of Jerusalem, Jerusalem, Israel

Key Points:

- Integrated phytoplankton concentration in the northern Gulf is driven by horizontal advection
- Surface and integrated bloom behave differently in the southern and northern ends of the Gulf
- Deep mixing causes light limitation in the deep mixed northern Gulf which inhibits integrated growth

Corresponding author: Hadar Berman, hadarberman@gmail.com

Abstract

Phytoplankton bloom in the Gulf of Elat/Aqaba was studied before mainly using one-dimensional models and observations from the northern Gulf. Thus, the spatial variability within the Gulf and the contribution of physical processes such as horizontal advection to the bloom have not yet been studied. Moreover, various factors such as light limitation are still debated. Here we used a three-dimensional coupled physical-ecological model for the Gulf of Elat/Aqaba to study the mechanisms for phytoplankton bloom throughout the Gulf. We found the southern surface bloom to be higher than the northern surface. In contrast, southern integrated bloom is lower than the northern bloom. These differences are due to spatial variations in the mixed layer depth, which is much deeper in the northern Gulf compared with the south. Moreover, horizontal advection controls phytoplankton integrated biomass during the bloom, a process often neglected when dealing with phytoplankton blooms. Finally, we found that light limits growth of the northern integrated bloom.

Plain Language Summary

Phytoplankton forms the base of the marine ecological system. Despite its importance, observing relevant processes and interpreting them is extremely complex. Phytoplankton are subject to both physical processes (e.g. currents and mixing) and internal ecological processes (e.g. growth and grazing). These processes are intermittent in time, highly nonlinear, inhomogeneous in space, and span a wide range of spatial and temporal scales. The phytoplankton bloom is a phenomena where phytoplankton concentration is enhanced rapidly. The mechanism for phytoplankton bloom initiation in the Gulf of Elat/Aqaba was studied before using a limited number of observations from a single station in the north, which is insufficient to understand spatial variability or the role of horizontal advection. We studied this phenomena in the Gulf using a 3D coupled physical-ecological model. We found that despite the small dimension of the Gulf, there is large spatial variability with significant differences between the north and south. The ecological processes that occur in a water column are not sufficient to cause the integrated bloom. The integrated phytoplankton bloom in the northern Gulf is driven by horizontal advection from the south. In addition, light limits phytoplankton growth in the deep mixed northern Gulf, contrarily to what was previously known.

1 Introduction

Phytoplankton blooms have been defined as rapid (order of days or weeks) phytoplankton biomass accumulation (Platt et al., 1991). They have been studied worldwide, and various hypotheses for bloom initiation have been proposed over the years (e.g. Sverdrup, 1953; Behrenfeld, 2010; Huisman et al., 1999; Smetacek & Passow, 1990; Chiswell et al., 2015; Mahadevan et al., 2012; Zarubin et al., 2017). Phytoplankton blooms can refer to two different quantities: surface (e.g. Sverdrup, 1953) and depth integrated (e.g. Behrenfeld, 2010). The former refers to an elevated concentration of phytoplankton in the surface water, and the latter refers to an elevated concentration in the whole water column. Each of these quantities have corresponding rates of change which govern their behaviour over time. These differences in defining the bloom are a cause for confusion and inconsistency when dealing with phytoplankton blooms and can lead to contradicting conclusions regarding the processes responsible for the bloom initiation (e.g. Behrenfeld & Boss, 2018; Chiswell et al., 2015; Zarubin et al., 2017).

One of the definitions used for phytoplankton blooms is a positive net growth rate for a sufficient period of time (O(days/weeks), depending on location) (see for example Behrenfeld & Boss, 2018; Sverdrup, 1953). The net growth is the sum of all processes affecting phytoplankton concentration. These are comprised of ecological processes such as growth, grazing and mortality, and of physical processes, such as horizontal advec-

tion and vertical mixing (Behrenfeld & Boss, 2018; Chiswell et al., 2015). Both physical and ecological processes are important for changes in phytoplankton concentration.

Phytoplankton net growth rates are commonly inferred by using in-situ or satellite observed chlorophyll or carbon (e.g. Behrenfeld, 2010; Zarubin et al., 2017; Chiswell et al., 2015; Behrenfeld & Boss, 2018). Although net growth rate does not distinguish between the different processes which control phytoplankton concentration, it is usually used to understand the bloom initiation mechanism since it is the main rate that can be estimated through observations. In order to do so, assumptions are made to neglect physical processes in an attempt to understand the bloom ecological drivers (e.g. Behrenfeld, 2010; Chiswell et al., 2015). Vertical mixing can be neglected when looking at surface bloom by presuming that phytoplankton concentration is vertically constant within the mixed layer (e.g. Chiswell et al., 2015). Vertical mixing cancels out in the integrated bloom when integrating over the whole water column. Horizontal advection, which is difficult to take into account, is also usually neglected by presuming a 1D domain (e.g. Chiswell et al., 2015) or by averaging over a large area (e.g. Behrenfeld, 2010). In this work we differentiate between the physical and ecological processes controlling the net growth rate in the Gulf of Elat/Aqaba (hereinafter **the Gulf**). We conclude that horizontal advection cannot be neglected as it is an important driver for winter integrated net growth rate in the Gulf.

As the effect of the 3D physics is complicated and hard to characterize through observations (Mahadevan, 2016) they are usually examined through numerical models. Eddies can influence the bloom by causing changes in mixing and stratification (e.g Mahadevan et al., 2012; Lévy et al., 1998; McGillicuddy et al., 1998). Horizontal advection is linked to spatial heterogeneity and phytoplankton patchiness (Mahadevan, 2016; Martin, 2003). The effect of horizontal advection as a diluting process can have a positive (due to dilution of grazers and viral infections) and negative (due to dilution of nutrients) effect on the phytoplankton production (Lehahn et al., 2017). Horizontal advection can have an important effect on biological populations by frontal systems or coastal upwelling (Daly & Smith Jr, 1993). Nutrient supply by horizontal advection was found to be dominant in the North Atlantic subtropical gyre (Oschlies, 2002). Harmful algal blooms in coastal upwelling regions can be controlled by the conditions in offshore waters instead of inshore waters where the bloom is measured due to horizontal advection processes (Donaghay & Osborn, 1997).

We employ a 3D coupled physical-ecological climatological model of the Gulf. This model enables us to distinguish between the processes controlling phytoplankton concentration. We confirm previous studies that showed that nutrient input has a major effect on phytoplankton surface and integrated bloom. Our new findings are: (1) spatial variability within the Gulf is large, in spite of its small dimensions (length of around 180 km); northern surface and integrated bloom is higher and lower than southern bloom, respectively; (2) while nutrients are the main limiting factor for integrated specific growth in the southern Gulf, light significantly limits integrated growth in the deep mixed northern Gulf; (3) integrated net growth rates in the Gulf are significantly affected by horizontal advection from the south, thus neglecting them can lead to incorrect conclusions.

This paper is organised as follows: in the rest of the introduction we provide an overview of the Gulf dynamics and ecological system (1.1). The model is described in Section 2. Methods used in the paper are detailed in Section 3. Results are detailed in Section 4 and are discussed in Section 5.

1.1 The Gulf of Elat

The Gulf is a deep (maximal depth 1800 m, mean 800 m. See Figure 1) elongated (180 X 5-25 km), and arid (net evaporation range between ∼1.8-3 m/y e.g. Ben-Sasson et al. (2009); Cohen et al. (1977); Biton and Gildor (2011b)) semi-enclosed basin, con-

nected to the Red Sea via the Straits of Tiran (maximal depth ∼250 m). The shallow depth of the straits prevents cold water from entering the Gulf, which results in relatively warm deep water in the Gulf.

Our knowledge of the Gulf dynamics is based on a limited number of observations and on numerical models. There are repeated monthly measurements in the northern Gulf in Station A (illustrated in Figure 1) by the National Monitoring Program (**NMP**, `https://iui-eilat.huji.ac.il/Research/NMPAbout.aspx`), which include temperature, salinity, pressure and irradiance profiles. High resolution measurements in the northern Gulf are conducted irregularly (Carlson et al., 2012, 2014). In the rest of the Gulf, observations are sporadic (Manasrah et al., 2006; Plähn et al., 2002; Manasrah et al., 2004). Numerical studies include simple models (Wolf-Vecht et al., 1992; T. Berman et al., 2003a; Silverman & Gildor, 2008; Badran et al., 2005) and general circulation models (T. Berman et al., 2000, 2003b; Brenner & Paldor, 2004; Biton & Gildor, 2011a, 2011b, 2011c).

Deep water is formed in winter, through shelf and open-water convection due to surface cooling (Wolf-Vecht et al., 1992; Genin et al., 1995; Biton et al., 2008). Mixing occurs in pulses, resulting from atmospheric forcing. The surface water in the Gulf is replaced by warm surface Red Sea water in the months after mixing (Biton & Gildor, 2011b). Stratification can also occur by rapid pulses of water masses with elevated temperature and is affected by short-lived eddies (Carlson et al., 2014). The advected water can have an important effect on the nutrient concentrations in the Gulf (Biton & Gildor, 2011c; Wolf-Vecht et al., 1992). Monthly averaged temperature and salinity observations from two stations in the north and south Gulf between 1974 to 1977 show weaker water column stratification in the northern Gulf compared with the southern Gulf in both winter and summer (Paldor & Anati, 1979).

Phytoplankton and nutrient dynamics have been studied in the northern Gulf using 1D numerical modeling (Kuhn et al., 2018) and observations (e.g. Lindell & Post, 1995; Genin et al., 1995; Al-Najjar et al., 2007; Labiosa et al., 2003); a limited number of observations were also conducted in the south (Levanon-Spanier et al., 1979; Al-Qutob et al., 2002; Stambler, 2005). The NMP collects monthly profiles of chlorophyll, nutrients, particulate organic carbon, zooplankton, oxygen, PH, and more from Station A and coastal stations. Chlorophyll a exhibits seasonal fluctuations, with low surface concentrations in summer, increased surface concentrations in winter and maximum surface concentrations in spring. During the mixing season the Gulf exhibits high integrated chlorophyll concentrations (e.g. Levanon-Spanier et al., 1979; Genin et al., 1995; Zarubin et al., 2017). Following winter mixing, which causes nutrient enrichment, there is an exceptionally high surface spring bloom compared with other subtropic oligotrophic basins (Zarubin et al., 2017). High surface chlorophyll concentration also follows winter mixing in the northern main body of the Red Sea, and is linked to the nutrient input from the deep water (Gittings, 2016).

The oligotrophic nature of the Gulf originates from input of nutrient depleted Red Sea surface water. The Gulf resembles other larger oligotrophic basins, specifically oligotrophic central masses, such as the Sargasso Sea (Levanon-Spanier et al., 1979; Reiss & Hottinger, 1984, Chapter 5). Phytoplankton growth in the Gulf can be limited by nitrogen alone (Levanon-Spanier et al., 1979) or co-limited by nitrogen and phosphorous (Suggett et al., 2009).

It is still debated whether light limits phytoplankton growth in the Gulf. Stambler (2006) claimed that due to the low turbidity of the water, light does not limit phytoplankton growth in the upper 100 m throughout the year. Moreover, during deep mixing periods phytoplankton do not show effects of photoacclimation, suggesting that during winter incident light does not limit growth in the whole water column (Stambler, 2006). Zarubin et al. (2017) noticed that net growth rates (inferred from observations) were highest during minimum incident light and thus concluded that incident light does not limit inte-

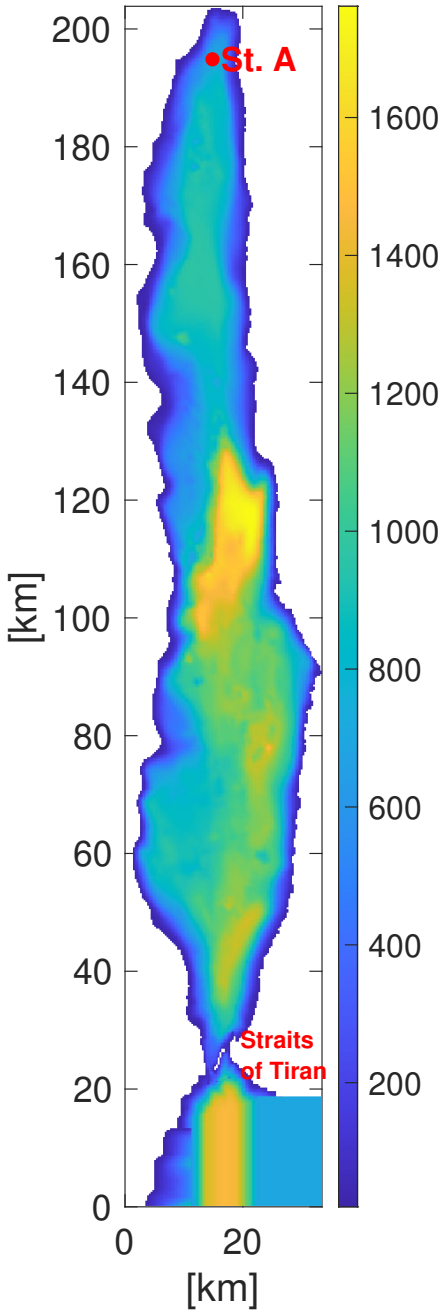

Figure 1. The domain of the model and the bathymetry of the Gulf. The Gulf is connected to the Red Sea through the Straits of Tiran in the south (more information in Section 1.1). NMP monthly observations take place in Station A in the northern Gulf. The location of the Straits of Tiran and Station A are illustrated.

grated phytoplankton growth in the Gulf and that phytoplankton are mostly limited by nutrients. In contrast, by using nitrogen budgets, Meeder (2012) found a decrease in integrated phytoplankton growth when mixing exceeded 550 m. Since nutrients are abundant throughout the water column when mixing exceeds 550 m and increased mixing depths are associated with light limitation (Gran & Braarud, 1935), Meeder (2012) suggested that light was the dominant limitation for growth when mixing exceeded this depth. Here we found that light availability is a dominant limitation for integrated growth during winter mixing in the northern Gulf.

Spatial variability of primary production and chlorophyll concentrations in the Gulf have been reported in the past. The Gulf exhibits east to west chlorophyll gradients, where the eastern side, which is characterized by upwelling (and thus higher nutrient supply compared with the western side), exhibits a larger phytoplankton concentration (Labiosa et al., 2003). Using observations from summer 1997, Rasheed et al. (2002) showed that chlorophyll concentration is lower in offshore stations ($\sim$3 km from shore $\sim$600 m deep), compared with inshore stations (up to $\sim$30 m deep $\sim$100 m from the Jordanian shore) by up to 0.2 μ g /l. This is in agreement with values reported by the NMP, which are higher in the pier station compared with Station A in summer. According to NMP data this difference is even more pronounced in winter, when surface values in the pier station range between 0.8-2 μ g /l while surface values in Station A rarely exceed 0.5 μ g /l. Differences in chlorophyll concentration and primary production between the southern and northern ends of the Gulf were reported by Levanon-Spanier et al. (1979). Occasional cruises between the years 1975-1977 show differences in chlorophyll and primary production vertical profiles between the northern and southern Gulf. The southern Gulf has high chlorophyll values ($\sim$15 km north of the Straits of Tiran, maximum values in the deep chlorophyll maximum of $\sim$0.7 μ g /l) compared with Station A in the north ($\sim$0.2 μ g /l) during winter (Levanon-Spanier et al., 1979). In addition, the southern Gulf shows a more stratified pattern than the northern Gulf during winter months (Levanon-Spanier et al., 1979). In this work we looked at the north-south spatial differences and analyzed the differences in the mechanisms which control phytoplankton growth in the southern and northern Gulf.

Despite the severe nutrient limitation, the Gulf exhibits an exceptional surface bloom compared with other oligotrophic areas (Labiosa et al., 2003). Exceptional cooling, and thus enhanced deep mixing conditions, causes stronger phytoplankton blooms (Genin et al., 1995). Theories for the mechanisms responsible for the bloom initiation were proposed and tested specifically for the Gulf. Meeder (2012) claimed that the integrated bloom initiates when mixing depth increases beyond 250 m which is the depth of the base of the nitracline. This threshold is sufficient for nutrient supply which limits phytoplankton growth during summer. If the MLD increases beyond 550 m, light becomes the limiting factor for integrated growth and the integrated bloom is inhibited. With the onset of stratification a rapid surface bloom occurs due to nutrient abundance and light availability. Zarubin et al. (2017) offered the dispersion-confinement mechanism for the bloom in the Gulf. In this hypothesis, high integrated net growth rate increases with MLD deepening due to nutrient enrichment. This high integrated net growth rate is compensated by dilution due to deep mixing (dilution phase), which results in constant chlorophyll concentration in the photic layer. Due to the high integrated net growth rates, the integrated chlorophyll increases to a maximum when mixing is maximum. Stratification (or the confinement phase) produces an increase in the surface chlorophyll concentration due to the lack of active mixing (or dilution), where they continue to grow until nutrient depletion.

2 Model description

2.1 Physical model

The model of the Gulf is based on the Massachusetts Institute of Technology General Circulation Model (**MITgcm,** Marshall, Adcroft, et al., 1997; Marshall, Hill, et al., 1997). The physical model for climatological conditions was previously used to study various dynamical processes in the Gulf (Biton & Gildor, 2011c, 2011a, 2011b, 2016). The model's domain includes the whole Gulf, ending 20 km south of the Straits of Tiran (See Figure 1). The horizontal resolution is 300 m with 32 vertical levels concentrated mostly in the upper 300 m. The model is a free-surface, hydrostatic primitive equation ocean model with a KPP mixing scheme (Large et al., 1997) suitable for unstable regimes. The horizontal viscosity is calculated using Smagorinsky scheme (Smagorinsky, 1963). There is no explicit horizontal diffusion, but tracer's horizontal eddy diffusivity is indirectly influenced by the advection scheme. An open boundary for the Straits of Tiran is used to relax temperature and salinity to climatological profiles (more information in Biton & Gildor, 2011b). The physical model was run for a period of 20 years to achieve quasi steady state.

2.2 Ecological model

The ecological model is a simplified Nutrient-Phytoplankton-Zooplankton-Detritus (NPZD) model, including one Phytoplankton (**P**, $[mmol - N/m^3]$) and Zooplankton species (**Z**, $[mmol - N/m^3]$), Nitrogen as the limiting nutrient (**N**, $[mmol - N/m^3]$) and Detritus (**D**, $[mmol - N/m^3]$). In addition, we included an equation to convert phytoplankton biomass to chlorophyll (**Chl**, $[\mu g/l]$), following Geider et al. (1997). The equations are based on Follows et al. (2007), but were altered to include processes shown to be significant in the Gulf. Model equations are detailed in equations 1-6. More details about the model equations and parameter optimization procedure can be found in Appendix 1.

$$\frac{DN}{Dt} = -\mu\frac{N}{N+k_{satN}}i_{lim}P + k_{min}D + m_{zn}Z + m_{pn}P + \frac{\partial}{\partial z}(K\frac{\partial N}{\partial z}) \tag{1}$$

$$\frac{DP}{Dt} = \mu\frac{N}{N+k_{satN}}i_{lim}P - g\frac{P^2}{P^2+k_{gsat}^2}Z - m_pP - m_{pn}P + \frac{\partial}{\partial z}(K\frac{\partial P}{\partial z}) \tag{2}$$

$$\frac{DZ}{Dt} = e_{eff}g\frac{P^2}{P^2+k_{gsat}^2}Z - m_{zn}Z - m_zZ^2 + \frac{\partial}{\partial z}(K\frac{\partial Z}{\partial z}) \tag{3}$$

$$\begin{aligned}\frac{DD}{Dt} &= m_pP + m_zZ^2 - k_{min}D + (1-e_{eff})g\frac{P^2}{P^2+k_{gsat^2}}Z \\ &\quad + w_{ns}\frac{\partial D}{\partial z} + \frac{\partial}{\partial z}(K\frac{\partial D}{\partial z})\end{aligned} \tag{4}$$

$$\begin{aligned}\frac{DCHL}{Dt} &= \rho_{chl/phy}\mu\frac{N}{N+k_{satN}}i_{lim}P - m_pCHL - g\frac{P^2}{P^2+k_{gsat^2}}Z\frac{CHL}{P} \\ &\quad - m_{pn}CHL + \frac{\partial}{\partial z}(K\frac{\partial CHL}{\partial z})\end{aligned} \tag{5}$$

The ecological model was forced by monthly mean surface Photosyntheticaly Active Radiation (**PAR**). The PAR data was retrieved from hourly data of surface PAR from the Interuniversity Institute for marine sciences in Elat (**IUI**) meteorological data (`http://www.meteo-tech.co.il/eilat-yam/eilat_download_en.asp`) in the period between 2011-2020. The southern boundary of the model is relaxed to nitrate observations from the northern Red Sea station 28862 downloaded from the WOA13 (`https://`

www.nodc.noaa.gov/cgi-bin/OC5/woa13/woa13oxnu.pl). Relaxation time for the boundary condition is one day. This is the only open boundary in the model, i.e. there is no accumulation of matter in the sediments.

All variables were initialised based on NMP data from December 2010 throughout the Gulf, although NMP data is only from the northern end, as there is no detailed data elsewhere. Nitrogen was initialized from combined data of nitrite and nitrate. Phytoplankton concentration was converted from chlorophyll units ($\mu g/l$) by using a value of 40 $mg-C/mg-Chl$ (Zarubin et al., 2017), the Redfield ratio (found to be similar to the N/P ratio in the Gulf by Häse et al. (2006)) and carbon molecular weight to get units of $mmol - N/m^3$. Zooplankton was taken as 10% of phytoplankton concentration in each depth (as in Lévy, 2015), as the NMP data does not provide depth resolution for zooplankton data. Detritus was taken from particulate organic carbon data of NMP and converted to $mmol-N/m^3$ using the Redfield ratio. The model was run for five years of spin up, and reached quasi steady state. The presented results are the sixth year run.

2.3 Model comparison to observations

Model comparison to chlorophyll, nitrogen and zooplankton NMP observations in Station A (taken from http://www.meteo-tech.co.il/EilatYam_data/ey_data.asp) are shown in figures 2, 3 and 4 respectively. Each month's data is an average over the years 2003-2020. Modeled chlorophyll structure showed reasonable agreement with the NMP observations. The deep chlorophyll maximum is apparent and occurs in a similar depth as in observations in summer months of June-August. The model nitrogen and chlorophyll vertical profiles are homogeneous in the mixed layer between November-March, in agreement with observations. Values of chlorophyll were lower in September-December in the model compared with NMP observations, although the structure is similar. This could be due to lower climatological PAR in these months compared with the values used for the optimization of these months in the years 2011-2012, or due to insufficient input of nutrients to the northern surface water by advection in the model. Nitrogen surface observations (0-200 m) show good resemblance to observed values. Intermediate values (200-500 m) differ from observations especially in the summer months. Deep (>500 m) values of nitrogen were similar between model and observations. We stress that the depths under 200 m were less important for phytoplankton production in summer. Modelled zooplankton exhibits a rise between February and May as in the NMP observations. Summer modeled values are relatively constant and lower than the observed values.

We compared the model upper 50 m mean chlorophyll results (optical depth to compare with MODIS in clear water as described in https://oceancolor.gsfc.nasa.gov/forum/oceancolor/topic_show.pl?tid=553) to climatological chlorophyll obtained from MODIS level 3 mapped 4km resolution (obtained from https://oceancolor.gsfc.nasa.gov/l3/) (Figure 5). The high surface chlorophyll concentration in winter is reproduced by the model and the north to south gradient can be seen (Figure 5 left panels). The summer chlorophyll values are low in both model and satellite observations (Figure 5 right panels). Model results agree with Levanon-Spanier et al. (1979) observation for north-south gradients in surface chlorophyll. Modeled Jan-Mar southern Gulf shows a maximum value of 0.6 μ g/l and north shows 0.2-0.3 μ g /l similar to what was showed by Levanon-Spanier et al. (1979) observations (see Section 1.1.

3 Calculations and definitions

3.1 Surface and integrated phytoplankton concentrations

We examined phytoplankton dynamics in the surface water and in the whole water column, using the following definitions:

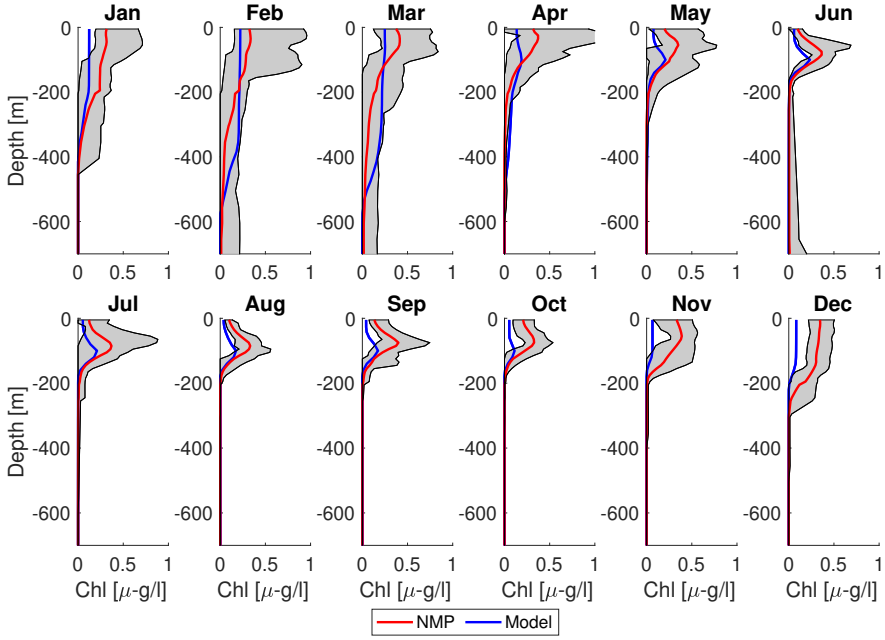

Figure 2. Observed (red) and simulated (blue) chlorophyll climatology profiles. Observations (red) are monthly means measured by the NMP in 2003-2020. Gray area represents the maximum and minimum profiles measured by the NMP.

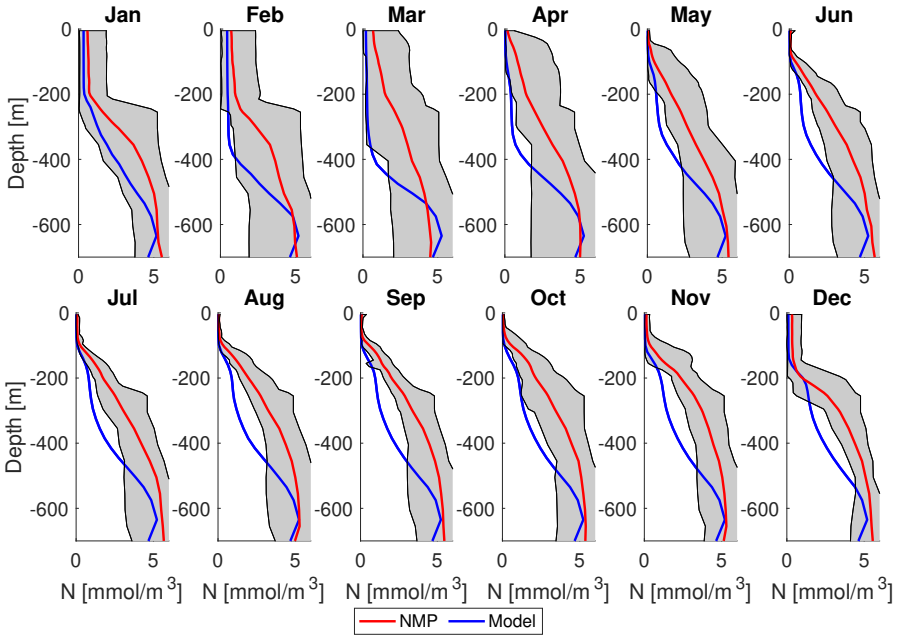

Figure 3. Observed (red) and simulated (blue) monthly means of nitrogen [$mmol\text{-}N/m^3$] measured by the NMP in 2003-2020. Gray area represents the maximum and minimum profiles measured by the NMP.

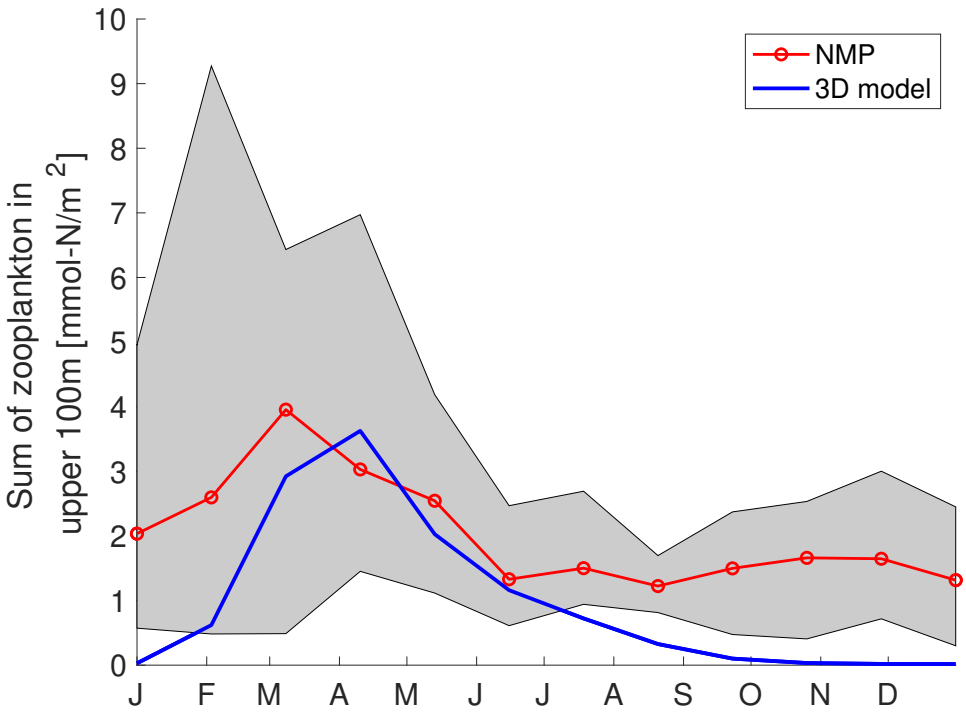

Figure 4. Observed (red) and simulated (blue) zooplankton integrated over the upper 100 m [$mmol\text{-}N/m^2$]. The gray area marks the maximum and minimum of the NMP observations. NMP measurements are between 2011-2020.

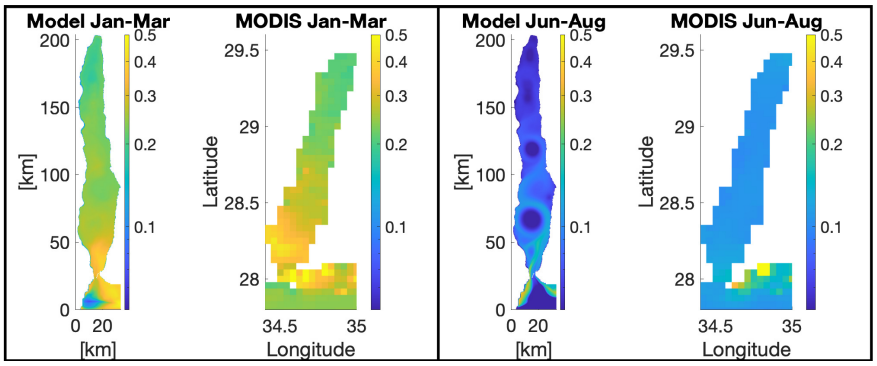

Figure 5. Surface chlorophyll as observed by MODIS-AQUA level 3 imagery compared with model simulations for mixing months (Jan-Mar, left panels) and stratified months (Jun-Aug, right panels).

Surface phytoplankton concentration $[mmol\text{-}N/m^3]$ was defined as the concentration in the upper layer of the model, which is 10 m deep. The results are insensitive to this specific depth and will yield the same conclusions when using 35 m deep as well.

Integrated phytoplankton concentration $[mmol\text{-}N/m^2]$ is calculated as the phytoplankton depth integration over the whole water column, i.e. as $\Sigma_{i=1}^{n} P_i \Delta z_i$, where P_i is the phytoplankton concentration in each depth (z_i) and $n = 32$ is the number of grid points in the water column.

3.2 Phytoplankton rates of change

Phytoplankton biomass rates of change $[1/d]$ are the measure of change in phytoplankton concentration in every given time and location, which is affected by both ecological and physical processes, normalized by phytoplankton concentration. We calculate various rates, as detailed below, to better understand the annual cycle of the ecological system and the bloom dynamics. Calculations of the integrated and surface rates are similar to Chiswell et al. (2015). The following defined rates are either surface or integrated rates as detailed below.

Surface rate $[1/d]$ is the rate of change in the model upper layer normalized by the phytoplankton concentration e.g. $\frac{1}{P_{i=1}} \frac{\partial P_{i=1}}{\partial t}$.

Depth integrated rate $[1/d]$ is the integrated rate over the whole water column divided by the integrated phytoplankton concentration. For example, the integrated net growth rate is calculated as: $\frac{1}{\Sigma_{i=1}^{n} P_i \Delta z_i} \Sigma_{i=1}^{n} \frac{\partial P_i}{\partial t} \Delta z_i$, (Similar to Chiswell, 2011).

Specific growth rate $[1/d]$ is the phytoplankton growth rate, which is dependent on nutrient and light limitation, divided by the phytoplankton concentration ($\frac{1}{P} \mu \frac{N}{N+k_{satN}} i_{lim} P$).

PAR limited growth rate $[1/d]$ is the specific growth rate if only light was limiting phytoplankton growth ($\frac{1}{P} \mu i_{lim} P$).

N limited growth rate $[1/d]$ is the specific growth rate if only nutrients were limiting phytoplankton growth ($\frac{1}{P} \mu \frac{N}{N+k_{satN}} P$).

Ecological growth rate $[1/d]$ is the sum of the ecological rates ($\frac{1}{P}(\mu \frac{N}{N+k_{satN}} i_{lim} P - g \frac{P^2}{P^2+k_{gsat}^2} Z - m_p P - m_{pn} P)$).

Physical rate $[1/d]$ is the sum of the advection and vertical mixing rates in the phytoplankton equation ($-\frac{1}{P} \vec{V} \vec{\nabla} P + \frac{1}{P} \frac{\partial}{\partial z}(K \frac{\partial P}{\partial z})$).

Net growth rate $[1/d]$, is the sum of all ecological and physical processes in the equation for P (phytoplankton), Equation 2. The net growth rate is composed of the specific growth rate ($\frac{1}{P} \mu \frac{N}{N+k_{satN}} i_{lim} P$), mortality ($-\frac{1}{P}(m_p + m_{pn}) P$), grazing ($-\frac{1}{P} g \frac{P^2}{P^2+k_{gsat}^2} Z$), advection and vertical mixing rates ($-\frac{1}{P} \vec{V} \vec{\nabla} P + \frac{1}{P} \frac{\partial}{\partial z}(K \frac{\partial P}{\partial z})$). Net growth rate determines the surface/integrated phytoplankton concentration in the surface/integrated water column.

3.3 Mixed layer depth

Previous studies (e.g. Franks, 2014; Chiswell, 2011; Huisman et al., 1999; Lévy, 2015) have shown the importance of using the Active Mixed Layer Depth (**AMLD**), as opposed to Mixed Layer Depth (**MLD**) calculated from temperature gradients, when dealing with the phytoplankton annual cycle. The AMLD takes into account the active mixing in the water column. We compared the differences between the AMLD calculated using two thresholds for the Eddy diffusivity: 10^{-4} and 10^{-2} m^2/s. The AMLD was set to be the

minimum depth in which Eddy diffusivity was larger than the threshold. According to Huisman et al. (1999), vertical eddy diffusivity can range between 10^{-2} (very turbulent water) and 10^{-5} (stratified conditions). As no significant difference was found between the two thresholds in terms of the depth of of the AMLD, we used the value of 10^{-2} m^2/s to calculate the AMLD.

3.4 Phytoplankton transport

Integrated normalized transport of phytoplankton from and into the three selected areas (as detailed below) were calculated for each time step using: $\frac{1}{\Sigma_{j=1}^{m}\Sigma_{i=1}^{n}P\Delta z_i\Delta x_j\Delta y}\Sigma_{j=1}^{m}\Sigma_{i=1}^{n}(P_{i,j}V_{i,j})\Delta z_i\Delta x_j$. Here V is the north-south velocity, m is the number of grid points in the east-west direction and Δy, the size of a grid cell in the north-south direction is equal to 300 m. The units of the normalized transport are therefore $1/d$.

4 Results

4.1 Surface and integrated phytoplankton

A Hovmoller diagram (Figure 6) shows the Gulf's annual variability of the zonal mean surface and integrated phytoplankton concentrations and AMLD. Two important results can be seen: 1. Surface (Figure 6a) phytoplankton concentration exhibits a negative (north to south) gradient during winter-spring. In contrast, integrated (Figure 6b) phytoplankton concentration exhibits a positive (south to north) gradient during winter-spring; and 2. Being a terminal basin, as expected, winter AMLD (Figure 6c) is much deeper in the northern end of the Gulf (maximum of 370 m) compared with the central and southern parts of the Gulf. While summer AMLD is nearly constant throughout the Gulf, AMLD deepening in the northern Gulf precedes that of the south. To demonstrate these results, we calculated mean values of surface and integrated chlorophyll and AMLD in three areas of the Gulf (areas illustrated in Figure 6 by white, black and red shading). The Northern Gulf (**NG**, includes station A, ∼145-175 km from the Straits of Tiran, maximum depth of ∼950 m), the Central Gulf (**CG**, ∼75-105 km from the Straits of Tiran, maximum depth of ∼1760 m) and the Southern Gulf (**SG**, ∼0-30 km north of the straits of Tiran, maximum depth of ∼1350 m). These areas are substantially different in their mixing regimes and surface and integrated phytoplankton concentration.

Figure 7 shows the AMLD, integrated and surface phytoplankton concentration in the NG, CG and SG. The winter AMLD is deepest in the NG reaching down to ∼280 m (note that this value is lower than the 370 m mentioned above due to averaging over the whole NG region), it is lowest in the SG reaching ∼50 m, and somewhere in between in the CG reaching down to ∼125 m. During early spring, surface phytoplankton concentrations (blue curves) are highest in the SG (∼0.5 $mmol - N/m^3$), lowest in the NG (∼0.35 $mmol - N/m^3$), and again, in between in the CG (∼0.4 $mmol - N/m^3$). In contrast, winter integrated phytoplankton concentration is highest in the NG (∼1.2 $mmol - N/m^3$), lowest in the SG (∼0.4 $mmol - N/m^3$), with intermediate values in the CG (∼0.7 $mmol - N/m^3$). Summer integrated phytoplankton concentration is somewhat higher than surface concentration as most of the summer phytoplankton is concentrated in the deep chlorophyll maximum (∼100 m) and not in the surface layer (Figure 2).

4.2 Processes governing phytoplankton dynamics

Mechanisms for phytoplankton dynamics were studied using the phytoplankton rates of change defined in subsection 3.2. In the stratified season between June-December, phytoplankton surface and integrated concentration does not change

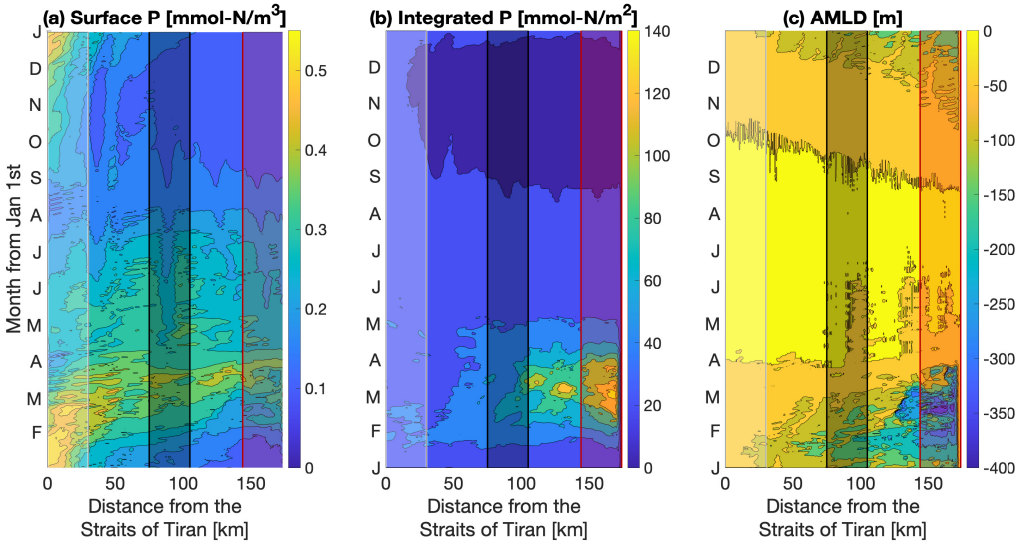

Figure 6. Hovmoller diagram: **(a)** Surface phytoplankton $[mmol - N/m^3]$; **(b)** Integrated phytoplankton $[mmol - N/m^2]$; and **(c)** AMLD [m] in the Gulf. X-axis is the distance from the Straits of Tiran [km] and y-axis is date from Jan 1st. The plotted surface and integrated phytoplankton and AMLD are zonal means. The shaded areas indicate the NG (red) the CG (black) and the SG (white).

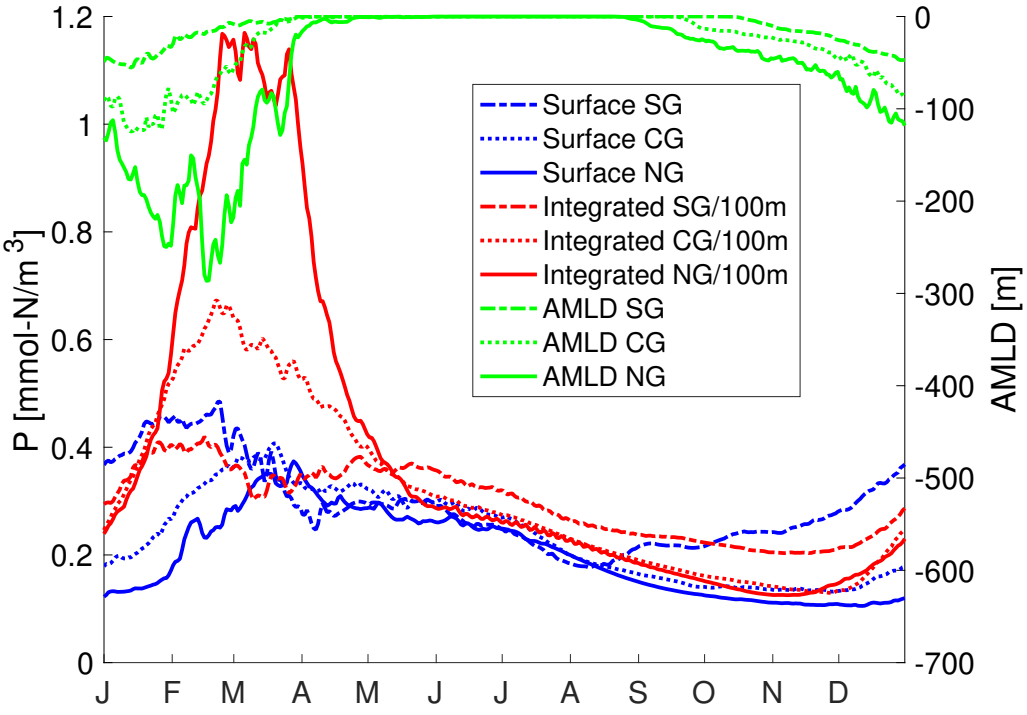

Figure 7. Surface (blue) and integrated (red) chlorophyll in three stations, NG (full line), CG (dotted line) and SG (dashed line) and their corresponding AMLD (green). Integrated chlorophyll is divided by 100 m to achieve the same units of $mmol - N/m^3$.

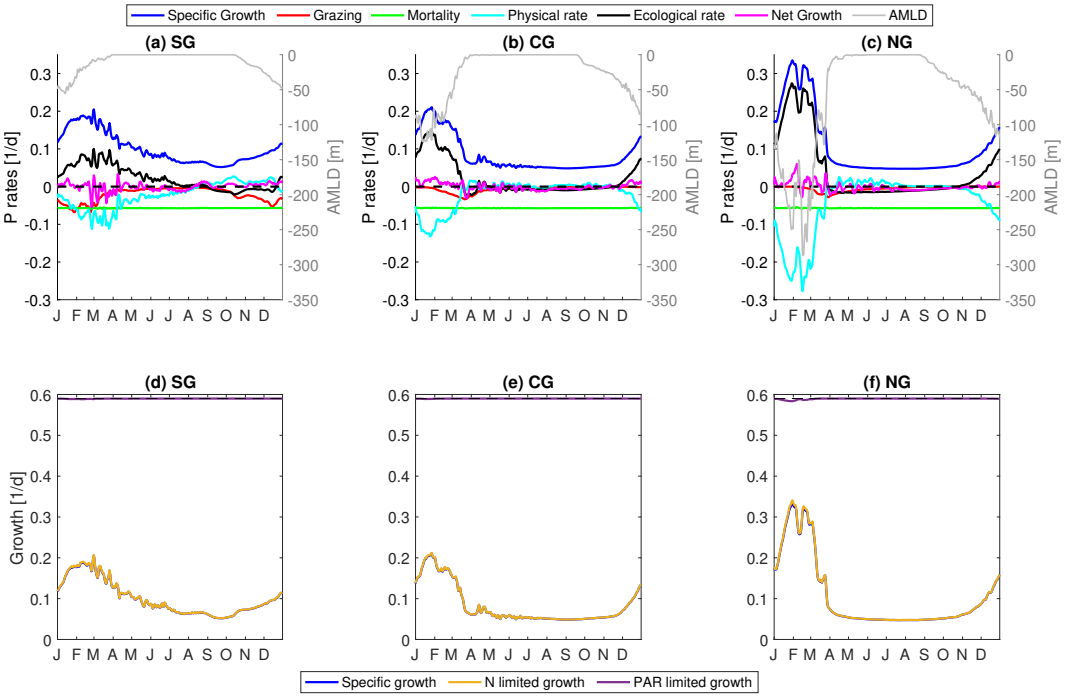

Figure 8. Upper panels: Phytoplankton surface rates in all three stations. Specific growth rate (blue, $\mu\frac{N}{N+k_{satN}}i_{lim}$), grazing rate (red, $g\frac{1}{P}\frac{P^2}{P^2+k_{gsat}^2}Z$), mortality rate (green, $(m_p + m_{pn})$), ecological growth rate (black, $\frac{1}{P}(\mu\frac{N}{N+k_{satN}}i_{lim}P - g\frac{P^2}{P^2+k_{gsat}^2}Z - m_pP - m_{pn}P)$), physical rate (cyan, $-\frac{1}{P}\vec{V}\vec{\nabla}P + \frac{1}{P}\frac{\partial}{\partial z}(K\frac{\partial P}{\partial z})$) and net growth rate (magenta, $\frac{1}{P}\frac{\partial P}{\partial t}$). AMLD is plotted in gray. **Lower panels:** Surface specific growth rates, if only nitrogen was limiting (orange, $\mu\frac{N}{N+k_{satN}}$), only PAR was limiting (purple, μi_{lim}) and real growth (blue, $\mu\frac{N}{N+k_{satN}}i_{lim}$). Black dashed line is the maximum growth possible in the water column (μ). Notice that the orange and blue lines almost completely coincide.

much (Figure 7), due to a near balance between the phytoplankton rates (explained below). Vertical mixing, followed by nutrient supply to the mixed layer, resulted in a rapid surface and integrated phytoplankton concentration increase. Net growth rate, composed of both ecological and physical rates, controls the phytoplankton concentration change - positive net growth rates may lead to a bloom. We note that ecological and physical rates can counteract each other, and even if the ecological rates are positive in a certain location promoting phytoplankton growth, physical processes can effect the net growth by counteracting the ecological processes and causing zero or negative net growth.

The surface ecological rates in summer were in a near balance between specific growth and mortality rates across the Gulf (Figure 8a-c). Other rates can be neglected in summer due to their small values (Figure 8a-c). The winter mixed layer deepening caused higher specific growth rate for surface phytoplankton concentration throughout the Gulf due to a decrease in nutrient limitation (orange curve in Figure 8d-f; higher values mean less limitation).

Winter surface specific growth rate (blue curves in Figure 8a-c) is highest in the NG (∼0.3 1/d), followed by the CG and the SG which show similar rates (∼0.2 1/d). Grazing (red curves in Figure 8a-c) is highest in the SG (∼0.06 1/d) followed by the CG (∼0.03 1/d) and the NG (∼0.02 1/d). Differences in grazing between the

areas are further discussed below. Physical processes act to decrease winter surface rates in all areas, in the NG and CG mostly due to vertical mixing of the surface layer with the deeper ones (can be seen to correspond with AMLD) while in the SG it is mainly due to horizontal advection.

The sum of all these rates, the surface net growth, is the rate that determines the surface phytoplankton trend. The net growth rate (magenta curves in Figure 8a-c) fluctuates around zero. Summer surface net growth rates are mainly a balance between specific growth and mortality, while in winter the balance is a combination of all rates, and the effect of the physical rate is important. The high winter specific growth rate (which is highest in the NG, blue curve 8c) is counteracted by the physical rates (cyan curve 8a-c) which are mainly due to vertical mixing in winter. Winter grazing is more dominant in the SG compared with the CG and NG (explained in more detail below).

As expected, Figure 8d-f shows that surface specific growth is limited in the surface only by nutrients since the N limited growth rate is almost identical to the specific growth rate. The nutrient limitation is weakest in the NG (i.e. N limited growth rate is higher) due to the deep mixing.

Similar to the summer ecological surface rates, the summer integrated ecological rates were in a near balance between specific growth and mortality rates across the Gulf (Figure 9a-c), while other ecological rates were negligible during summer. The winter mixed layer deepening caused higher specific growth for integrated phytoplankton concentration in the SG due to increased nutrients in the mixed layer depth (orange curve in Figure 9d; higher values mean less limitation), but not as much for the CG (Figure 9e) and NG (Figure 9f) due to light limitation, as will be explained below.

Integrated winter specific growth rates (Figure 9a-c) show the highest values in the SG ($\sim$0.13 1/d), followed by the CG ($\sim$0.07 1/d) and the NG ($\sim$0.06 1/d). Surprisingly, the integrated ecological rate in the NG and CG was positive only for a short period of time in the beginning of winter (Jan/Dec-Feb). Negative ecological rate in the NG winter is mostly driven by low specific growth rate (explained below). The high integrated phytoplankton concentration in the NG was driven by the advection rate (the physical rate is composed only of advection in the integrated rates). Thus the integrated high phytoplankton concentration is not created in the NG due to ecological processes, but is advected there from areas which do promote ecological growth.

To demonstrate the previous point, and show that winter phytoplankton is advected to the NG, depth integrated transport into the NG, out of the SG and into and out of the CG were calculated (as detalied in Section 3.4). The transport of phytoplankton can be seen in Figure 10. As was shown with the physical rate, the transport shows that SG outflow transport is large, CG input and output transport are similar to each other and approximately cancel out, while NG inflow is large in winter months between January-April. Thus, in our model most of the integrated phytoplankton into the NG is advected from the SG.

As opposed to the surface specific growth, which decreases from north to south, the integrated specific growth decreases from south to north. Although the N limited growth (orange curve in Figure 9f) is higher in the integrated NG (similar to what was found in the surface), the PAR limitation is significant. Thus the PAR limited growth (purple curves in 9d-e) is very low causing the specific growth rate to decrease. Southwards in the CG and more so in the SG, although nutrients were more limiting compared with the NG (orange curves in 9d-e), the light limitation (purple curves in 9d-e) decreased due to the shallow mixing depth. Thus we found

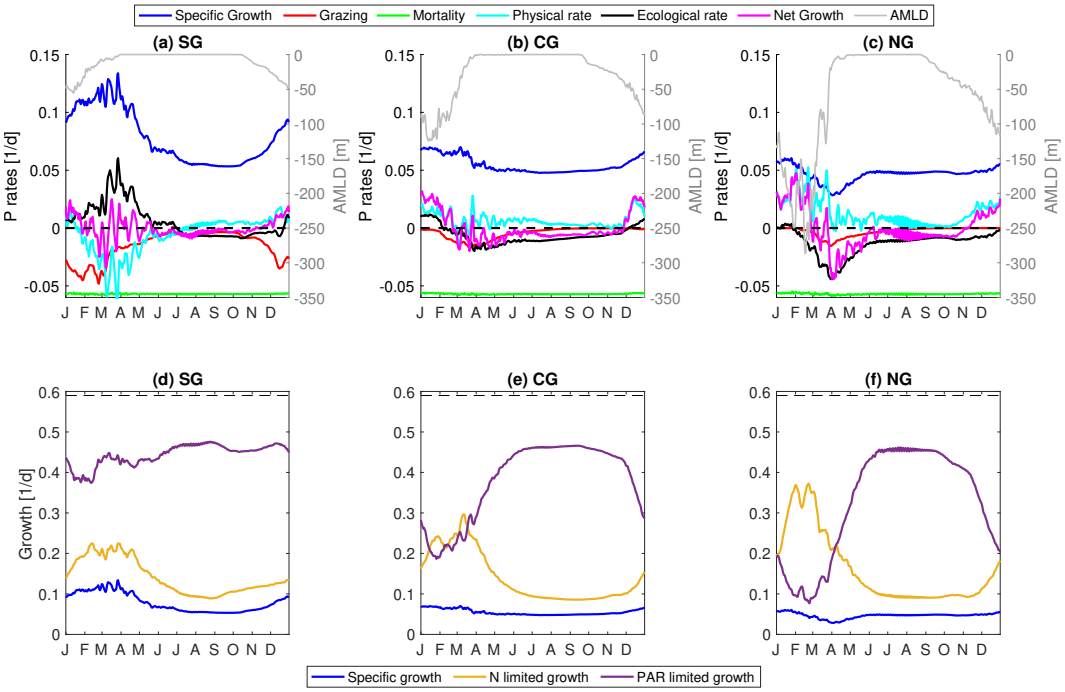

Figure 9. Upper panels: Phytoplankton integrated rates in all three stations. Specific growth rate (blue, $\mu \frac{N}{N+k_{satN}} i_{lim}$), grazing rate (red, $g \frac{1}{P} \frac{P^2}{P^2+k_{gsat}^2} Z$), mortality rate (green, (m_p+m_{pn})), ecological growth rate (black, $\frac{1}{P}(\mu \frac{N}{N+k_{satN}} i_{lim} P - g \frac{P^2}{P^2+k_{gsat}^2} Z - m_p P - m_{pn} P)$), physical rate (cyan, $-\frac{1}{P}\vec{V}\vec{\nabla}P + \frac{1}{P}\frac{\partial}{\partial z}(K\frac{\partial P}{\partial z})$) and net growth rate (magenta, $\frac{1}{P}\frac{\partial P}{\partial t}$). AMLD is plotted in gray. **Lower panels:** Integrated specific growth rates, if only nitrogen was limiting (orange, $\mu \frac{N}{N+k_{satN}}$), only PAR was limiting (purple, μi_{lim}) and real growth (blue, $\mu \frac{N}{N+k_{satN}} i_{lim}$). Black dashed line is the maximum growth possible in the water column (μ).

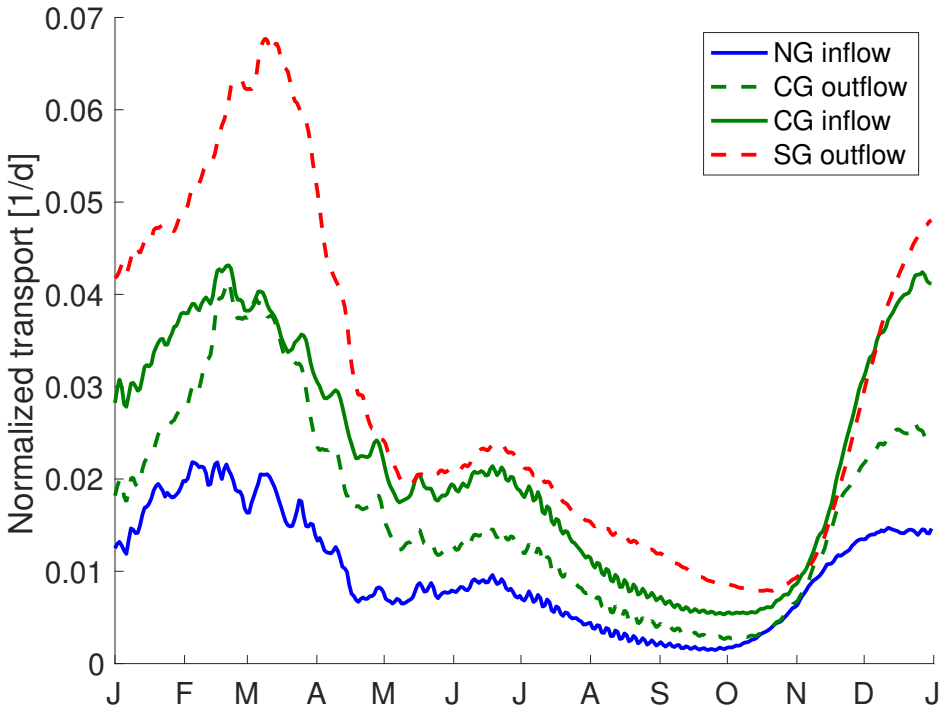

Figure 10. Input and output transports of phytoplankton to and from the NG, SG and CG areas [1/d]. Solid lines represent transport into the area and dashed lines represent transport out of the area. Positive transports are northwards.

that the effect of light limitation is more dominant in the NG and decreases southwards due to the varying mixing depth. This increased light limitation in the NG overcomes the nutrient limitation causing the specific growth to be higher in the SG rather than in the NG. NG specific growth rate also exhibits a minima around April due to a combination of high light limitation and high nutrient limitation (Figure 9f).

Both surface and integrated grazing in the NG and CG were highest in the late winter/spring. Integrated grazing rates preceded surface grazing, corresponding in these stations to the preceding integrated compared with surface phytoplankton concentration. We found that the grazing rate is more important in the SG in both surface and integrated rates, compared with the other stations. Surface grazing is more dominant in the SG, as the surface phytoplankton and zooplankton concentration is higher, causing both the ratio between zooplankton and phytoplankton concentration to be higher and the $\frac{P^2}{P^2+k_{gsat}^2}$ to be higher in the SG compared with the NG. Integrated grazing was also higher in the SG compared with the NG, but for a different reason. Integrated grazing is harder to understand because the term $\frac{P^2}{P^2+k_{gsat}}\frac{Z}{P}$ cannot be separated due to the integration. However we found that the integrated value of $\frac{P^2}{P^2+k_{gsat}}Z$ was similar in the SG and in the NG, and the cause for the large spatial differences in integrated grazing rates (Figure 9a-c, red curves) is due to the high integrated P in the NG, which decreases $\frac{P^2}{P^2+k_{gsat}}\frac{Z}{P}$ in the NG. Thus, while grazing was similar in units of $mmol \quad - \quad Nm^{-3}$, we found that its rate in units of d^{-1} was considerably lower in the NG due to the amount of phytoplankton. The high specific growth was correlated with the high specific grazing in the SG. The specific grazing has been shown to increase with increasing specific growth before (Burkill et al., 1987). When specific grazing was very low, zooplankton concentration was also very low.

We conclude that winter surface phytoplankton specific growth is mostly balanced by vertical mixing. Nutrients are the main limitation for specific growth in the surface water, while the limitation is weaker in the NG compared with the CG and SG due to the deeper mixing and thus higher nutrient concentration. Integrated phytoplankton ecological rate is barely promoted in the NG (only for a short period of time in January). Horizontal advection played a dominant role in adding phytoplankton to the NG from the SG. The integrated specific growth is highest in the SG, since light limitation there is lowest, even though the NG is richer in nutrients, since light limitation there is stronger.

5 Discussion

Phytoplankton spatial variability in the Gulf has not been studied much in the past, although differences in the magnitude of phytoplankton biomass between the northern and southern Gulf have been reported before (Levanon-Spanier et al., 1979). Here we study for the first time, using a 3D physical-ecological model the mechanisms behind the inverse behavior between the surface and integrated phytoplankton biomass magnitudes.

Our results, which show that phytoplankton is limited by nutrients in winter both in surface and integrated rates, agree with previous work done in the Gulf (Zarubin et al., 2017; Meeder, 2012). We found that when the ecological rate was positive, specific growth rate was enhanced by nutrient enrichment. As in the dispersion-confinement mechanism (Zarubin et al., 2017), the dilution effect limits the phytoplankton concentration in surface water during winter and the timing of the integrated bloom initiation corresponds to mixed layer deepening.

While nutrients were the cause for growth enhancement in winter, we found that light limits growth in the well-mixed NG. Previous studies claimed that light was not a limiting factor for phytoplankton growth in the Gulf (Stambler, 2006; Zarubin et al., 2017). Meeder (2012) suggested a CD that inhibited the integrated bloom due to light. Our model results agree with Meeder (2012) that light was a limitation on the winter growth. Although from the integrated phytoplankton concentration it seemed that light was not a limiting factor, as integrated phytoplankton was sustained during winter, we found that the phytoplankton population increase in the NG was due to horizontal advection from the SG as opposed to high specific growth.

As opposed to previous work done in the Gulf, we showed that horizontal advection plays a significant role in the Gulf's phytoplankton dynamics. It is nearly impossible to reach this conclusion by observations alone. Inferring net growth rates from phytoplankton concentrations, which is popular in the literature when using in situ or satellite data (e.g. Behrenfeld, 2010; Zarubin et al., 2017), does not necessarily represent the ecological rates. As shown here, net growth rates can be dominated by physical processes, and thus do not represent the ecological growth rate.

To conclude, we found that even in the relatively small Gulf, spatial differences are significant. Nutrient input from the deep waters was essential for phytoplankton population to increase, however light inhibited integrated specific growth in areas with deep mixing conditions. Although limited by light, integrated phytoplankton concentration can still increase in deep mixing conditions due to horizontal advection from more productive areas. In a subsequent paper (H. Berman & Gildor, in prep) we show that these differences are enhanced by increased cooling. Further study should examine other effects on phytoplankton dynamics such as the effect of viruses.

Appendix A Ecological model

Nutrient limitation on growth was modeled as a michaelis-menten equation. The nutrient limited growth is therefore $Pm = \mu\frac{N}{N+k_{satN}}$. Light limitation effect on phytoplankton growth ($ilim$, e.g. in Eq. 2) was modeled as $ilim = (1 - exp(-\alpha_{chl}PAR\theta/Pm))$ (Geider et al., 1997, eq. 1) where θ is the chl-c ratio, Pm is nutrient limited growth (see above), PAR is the amount of light and α_{chl} is the initial slope of the PI curve normalized to chlorophyll.

The model includes 15 parameters detailed in Table A1. Model parameters were optimized using a genetic algorithm. Genetic algorithms are widely used for optimization of dynamical models in general and specifically for NPZD models (e.g Rückelt, 2010; Schartau & Oschlies, 2003; Kuhn et al., 2018). The genetic algorithm searches for parameter values which result in the maximum fitness, which is the inverse of the cost function (error). The optimization was run on a simplified 1D offline model (only depth) in order to reduce computational time. The optimization was run on the period between 1/12/2010-30/11/2012, one year of shallow mixing and one year of deep mixing. Diffusivity values were read from the 3D physical model (KPP coefficients). The cost function compared model output of chlorophyll, nitrogen and zooplankton to monthly data collected by the NMP in the years 2011 and 2012.

The algorithm creates 24 "chromosomes" in each generation, which contain a combination of the parameters in binary form. The next generation is composed partially by "mating" (taking part of two chromosomes) of the best fits and partially by random "mutation". The GA worked on 13 parameters for 600 generations in realistic ranges (as can be found in Table A1). The GA searches for the maximum

Table A1. Parameters of the NPZD model. The first 13 parameters were optimized in the ranges found in literature. The optimized value is detailed in the last column. The two bounded parameters are detailed in the last two rows.

Param	Units	Parameter explanation	Range	Ref	Best fit
k_{min}	d^{-1}	Remineralization rate	0.003-0.15	a,b	0.0042
m_{zn}	d^{-1}	Z excretion rate	0.01-0.35	c,d	0.066
μ	d^{-1}	P maximum growth rate	0.2-3	b,e	0.59
k_{satN}	$mmol\text{-}Nm^{-3}$	N half saturation coefficient	0.01-3.5	d,e	0.35
g	d^{-1}	Maximum grazing rate	0.1-4	c,d,e	3.5
k_{gsat}	$mmol\text{-}Nm^{-3}$	Grazing half saturation coefficient	0.1-5	c,d,e	1.6
m_p	d^{-1}	P mortality rate	0.01-0.25	d	0.02
m_{pn}	d^{-1}	P respiration rate	0.005-0.25	d	0.037
m_z	$(mmol\text{-}Nm^{-3})^{-1}d^{-1}$	Z mortality rate	0.01-1	b	0.97
e_{eff}	non-dimensional	Grazing efficiency	0.5-1		0.76
w_{ns}	md^{-1}	PON sinking rate	0.0024-20	e	0.2
α_{chl}	$mmol\text{-}N\mu g\text{-}chl^{-1}$ $m^2\mu E^{-1}$	Initial slope of the PI curve normalized to chlorophyll	$(0.18\text{-}3.15)\cdot 10^{-7}$	f	$0.77\cdot 10^{-7}$
θ_m	$\mu g{-}chl\cdot mmol\text{-}N^{-1}$	Maximum chl to N ratio	0.4-5.72	f	2.1
k_c	$m^3\cdot mg\text{-}chl^{-1}$	Light attenuation due to P	$6.7\cdot 10^{-4}$	g	-
k_0	m^{-1}	Clear-water attenuation coefficient	0.04	h	-

[a]Follows et al. (2007)
[b]Schartau and Oschlies (2003)
[c]Kuhn et al. (2018)
[d]Kuhn et al. (2015)
[e]Evans and Garçon (1997, chapter 8)
[f]Geider et al. (1997)
[g]Dishon et al. (2012)
[h]Stambler (2006)

Table A2. GA parameters used for optimization procedure.

GA Parameter	Description	Value
Precision	Number of values tested between range of parameters	10 bit or 1024 values
Chromosome length	Number of parameters to be optimized	13
Number of chromosomes	Number of sets of parameters	24
Number of generations	Number of generations to run the optimization	600
Probability for crossover	Probability to mate	0.5
Probability for mutation	Probability for mutation	0.01
Restart with elitism	Difference between all chromosome fitness is less than	20%

fitness, which is the inverse of the cost function (error). If the GA converges and fitness does not differ by 20%, the model parameters are initialized from random values, while the best set of parameters are saved (elitism). The GA parameters are detailed in Table A2.

The cost function was composed of the vertical sum of the common logarithm of the squared errors for each of the variables - chlorophyll a, nitrate and zooplankton, which are then summed up. The reasoning behind taking the logarithm is that the chlorophyll distribution is skewed. Thus, by taking the logarithm of chlorophyll, the distribution becomes less skewed and the squared error was then represented more correctly. We added a constant of 0.02 to all measurements to avoid zero values. This was then done to all the variables that were being optimized. Thus, the cost function was:

$$Cost = \sum_{l=1}^{L} \frac{1}{T} \sum_{j=1}^{T} \sum_{k=1}^{D} [log_{10}(\frac{C_{l,j,k}^{obs}}{\omega} + 0.02)^2 - log_{10}(\frac{C_{l,j,k}}{\omega}^{mod} + 0.02)^2] \quad \text{(A1)}$$

Where $C_{l,j,k}$ is the compared variable l (Chl, N and Z) in time j and depth k. C^{obs} denotes the observation and C^{mod} denotes the model result. ω is a weight factor with same units as the compared variable and was found after trial and error best suitable to be one for all optimized variables. L is the number of variables optimized in the process and is equal to three. T is the number of measurements (number of months) and D is the number of depths. Each variable was normalized to T. T is equal to 24 for chlorophyll and nitrogen and 21 for zooplankton since these are the data available in the NMP. Zooplankton has a lower influence on the cost function because the cost function is not divided by number of measurements (zooplankton data is depth integrated). The cost function was constructed in this way since nitrogen and chlorophyll observations are more accurate than zooplankton data, which can represent also predators in higher trophic levels.

Monthly measurements collected by the NMP during the period December 2010 to November 2012 were used for the optimization procedure. Depth profiles of chlorophyll a and nitrogen (nitrate and nitrite) from Station A, as well as zooplankton in the upper 100 m, were used for the optimization algorithm. Zooplankton AFDW (Ash Free Dry Weight) is converted to organic carbon using 50% of the AFDW (Salonen et al., 1976).

Acknowledgments

HB thanks the Eshkol foundation administered by the Israel Ministry of Science and Technology (MOST) for providing her PhD fellowship under grant number 0399587. Additional travel funding was provided to HB by the Mediterranean Sea Research Center of Israel. We would like to thank the Israel National Monitoring Program of

the Gulf of Elat (NMP) and NASA's Moderate-resolution Imaging Spectroradiometer (MODIS) for data provided to conduct this study.

References

Al-Najjar, T., Badran, M. I., Richter, C., Meyerhoefer, M., & Sommer, U. (2007). Seasonal dynamics of phytoplankton in the Gulf of Aqaba, Red Sea. *Hydrobiologia*, *579*(1), 69–83.

Al-Qutob, M., Häse, C., Tilzer, M. M., & Lazar, B. (2002). Phytoplankton drives nitrite dynamics in the Gulf of Aqaba, Red Sea. *Marine Ecology Progress Series*, *239*, 233–239.

Badran, M. I., Rasheed, M., Manasrah, R., & Al-Najjar, T. (2005). Nutrient flux fuels the summer primary productivity in the oligotrophic waters of the Gulf of Aqaba, Red Sea. *Oceanologia*, *47*(1).

Behrenfeld, M. J. (2010). Abandoning Sverdrup's critical depth hypothesis on phytoplankton blooms. *Ecology*, *91*(4), 977–989.

Behrenfeld, M. J., & Boss, E. S. (2018). Student's tutorial on bloom hypotheses in the context of phytoplankton annual cycles. *Global Change Biology*, *24*(1), 55-77. doi: 10.1111/gcb.13858

Ben-Sasson, M., Brenner, S., & Paldor, N. (2009). Estimating air-sea heat fluxes in semienclosed basins: The case of the Gulf of Elat (Aqaba). *Journal of Physical Oceanography*, *39*(1), 185–202.

Berman, H., & Gildor, H. (in prep). Inter-annual variability in phytoplankton and nutrients in the Gulf of Elat.

Berman, T., Paldor, N., & Brenner, S. (2000). Simulation of wind-driven circulation in the Gulf of Elat (Aqaba). *Journal of Marine Systems*, *26*(3), 349–365.

Berman, T., Paldor, N., & Brenner, S. (2003a). Annual SST cycle in the Eastern Mediterranean, Red Sea and Gulf of Elat. *Geophysical Research Letters*, *30*(5).

Berman, T., Paldor, N., & Brenner, S. (2003b). The seasonality of tidal circulation in the Gulf of Elat. *Israel Journal of Earth Sciences*, *52*(1), 11–19.

Biton, E., & Gildor, H. (2011a). The coupling between exchange flux through a strait and dynamics in a small convectively driven marginal sea: The Gulf of Aqaba (Gulf of Eilat). *Journal of Geophysical Research*, *116*(C6), 10.1029/2011JC006944.

Biton, E., & Gildor, H. (2011b). The general circulation of the Gulf of Aqaba (Gulf of Eilat) revisited: The interplay between the exchange flow through the Straits of Tiran and surface fluxes. *Journal of Geophysical Research*, *116*(C8), 10.1029/2010JC006860.

Biton, E., & Gildor, H. (2011c). Stepwise seasonal restratification and the evolution of salinity minimum in the Gulf of Aqaba (Gulf of Eilat). *Journal of Geophysical Research*, *116*(C8), 10.1029/2011JC007106.

Biton, E., & Gildor, H. (2016). On the origin of a chain of eddies in the Gulf of Eilat/Aqaba. *Journal of Physical Oceanography*, *46*(8), 2269 - 2284. doi: 10.1175/JPO-D-15-0208.1

Biton, E., Silverman, J., & Gildor, H. (2008). Observations and modeling of a pulsating density current. *Geophysical Research Letters*, *35*(14), 10.1029/2008GL034123.

Brenner, S., & Paldor, N. (2004). High-resolution simulation with the Princeton Ocean Model. *Int Expert Team Proj*, *6*.

Burkill, P., Mantoura, R., Llewellyn, C., & Owens, N. (1987). Microzooplankton grazing and selectivity of phytoplankton in coastal waters. *Marine biology*, *93*(4), 581–590.

Carlson, D., Fredj, E., & Gildor, H. (2014). The annual cycle of vertical mixing and restratification in the Northern Gulf of Eilat/Aqaba (Red Sea) based on high

temporal and vertical resolution observations. *Deep Sea Research*, *84*, 1–17.

Carlson, D., Fredj, E., Gildor, H., Biton, E., Steinbuck, J., Monismith, S., & Genin, A. (2012). Observations of tidal currents in the Northern Gulf of Eilat/Aqaba (Red Sea). *Journal of Marine Systems*, *102*, 14–28.

Chiswell, S. M. (2011). Annual cycles and spring blooms in phytoplankton: Don't abandon Sverdrup completely. *Marine ecology progress series*, *443*, 39–50.

Chiswell, S. M., Calil, P. H., & Boyd, P. W. (2015). Spring blooms and annual cycles of phytoplankton: A unified perspective. *Journal of Plankton Research*, *37*(3), 500-508. doi: 10.1093/plankt/fbv021

Cohen, Y., Krumbein, W. E., Goldberg, M., & Shilo, M. (1977). Solar Lake (Sinai). 1. Physical and chemical limnology 1. *Limnology and Oceanography*, *22*(4), 597–608.

Daly, K. L., & Smith Jr, W. O. (1993). Physical-biological interactions influencing marine plankton production. *Annual Review of Ecology and Systematics*, *24*(1), 555–585.

Dishon, G., Dubinsky, Z., Caras, T., Rahav, E., Bar-Zeev, E., Tzubery, Y., & Iluz, D. (2012). Optical habitats of ultraphytoplankton groups in the Gulf of Eilat (Aqaba), Northern Red Sea. *International journal of remote sensing*, *33*(9), 2683–2705.

Donaghay, P. L., & Osborn, T. R. (1997). Toward a theory of biological-physical control of harmful algal bloom dynamics and impacts. *Limnology and Oceanography*, *42*(5 part 2), 1283-1296. doi: https://doi.org/10.4319/lo.1997.42.5_part_2.1283

Evans, G. T., & Garçon, V. C. (1997). *One-dimensional models of water column biogeochemistry.*

Follows, M. J., Dutkiewicz, S., Grant, S., & Chisholm, S. W. (2007). Emergent biogeography of microbial communities in a model ocean. *Science*, *315*(5820), 1843–1846.

Franks, P. J. S. (2014, 10). Has Sverdrup's critical depth hypothesis been tested? Mixed layers vs. turbulent layers. *ICES Journal of Marine Science*, *72*(6), 1897-1907. doi: 10.1093/icesjms/fsu175

Geider, R. J., MacIntyre, H. L., & Kana, T. M. (1997). Dynamic model of phytoplankton growth and acclimation: Responses of the balanced growth rate and the chlorophyll a: carbon ratio to light, nutrient-limitation and temperature. *Marine Ecology Progress Series*, *148*, 187–200.

Genin, A., Lazar, B., & Brenner, S. (1995). Vertical mixing and coral death in the Red-Sea following the eruption of Mount-Pinatubo. *Nature*, *377*, 507–510.

Gittings, J. (2016). *Climate warming and interannual variability of phytoplankton phenology in the Northern Red Sea* (Unpublished doctoral dissertation).

Gran, H. H., & Braarud, T. (1935). A quantitative study of the phytoplankton in the Bay of Fundy and the Gulf of Maine (including observations on hydrography, chemistry and turbidity). *Journal of the Biological Board of Canada*, *1*(5), 279–467.

Häse, C., Al-Qutob, M., Dubinsky, Z., Ibrahim, E., Lazar, B., Stambler, N., & Tilzer, M. (2006). A system in balance?? Implications of deep vertical mixing for the nitrogen budget in the northern Red Sea, including the Gulf of Aqaba (Eilat). *Biogeosciences Discussions*, *3*(2), 383–408.

Huisman, J., van Oostveen, P., & Weissing, F. J. (1999). Critical depth and critical turbulence: Two different mechanisms for the development of phytoplankton blooms. *Limnology and Oceanography*, *44*(7), 1781–1787.

Kuhn, A. M., Fennel, K., & Berman-Frank, I. (2018). Modelling the biogeochemical effects of heterotrophic and autotrophic N_2 fixation in the Gulf of Aqaba (Israel), Red Sea. *Biogeosciences*, *15*(24), 7379–7401.

Kuhn, A. M., Fennel, K., & Mattern, J. P. (2015). Model investigations of the North Atlantic spring bloom initiation. *Progress in Oceanography*, *138*, 176–193.

Labiosa, R. G., Arrigo, K. R., Genin, A., Monismith, S. G., & van Dijken, G. (2003). The interplay between upwelling and deep convective mixing in determining the seasonal phytoplankton dynamics in the Gulf of Aqaba: Evidence from SeaWiFS and MODIS. *Limnology and oceanography*, *48*(6), 2355–2368.

Large, W. G., Danabasoglu, G., Doney, S. C., & McWilliams, J. C. (1997). Sensitivity to surface forcing and boundary layer mixing in a global ocean model: Annual-mean climatology. *Journal of Physical Oceanography*, *27*(11), 2418–2447.

Lehahn, Y., Koren, I., Sharoni, S., d'Ovidio, F., Vardi, A., & Boss, E. (2017). Dispersion/dilution enhances phytoplankton blooms in low-nutrient waters. *Nature communications*, *8*(1), 1–8.

Levanon-Spanier, I., Padan, E., & Reiss, Z. (1979). Primary production in a desert-enclosed sea—the Gulf of Elat (Aqaba), Red Sea. *Deep Sea Research Part A. Oceanographic Research Papers*, *26*(6), 673–685.

Lindell, D., & Post, A. (1995). Ultraphytoplankton succession is triggered by deep winter mixing in the Gulf of Aqaba (Eilat), Red Sea. *Limnology and Oceanography*, *40*, 1130-1141.

Lévy, M. (2015). Exploration of the critical depth hypothesis with a simple NPZ model. *ICES Journal of Marine Science*, *72*(6), 1916-1925. doi: 10.1093/icesjms/fsv016

Lévy, M., Mémery, L., & Madec, G. (1998). The onset of a bloom after deep winter convection in the Northwestern Mediterranean Sea: mesoscale process study with a primitive equation model. *Journal of Marine Systems*, *16*(1), 7-21. doi: https://doi.org/10.1016/S0924-7963(97)00097-3

Mahadevan, A. (2016). The impact of submesoscale physics on primary productivity of plankton. *Annual Review of Marine Science*, *8*(1), 161-184. (PMID: 26394203) doi: 10.1146/annurev-marine-010814-015912

Mahadevan, A., D'Asaro, E., Lee, C., & Perry, M. (2012). Eddy-driven stratification initiates North Atlantic spring phytoplankton blooms. *Science*, *337*(6090), 54–58.

Manasrah, R., Badran, M., Lass, H., & Fennel, W. (2004). Circulation and winter deep-water formation in the Northern Red Sea. *Oceanologia*, *46*(1), 5–23.

Manasrah, R., Lass, H., & Fennel, W. (2006). Circulation in the Gulf of Aqaba (Red Sea) during winter—spring. *Journal of oceanography*, *62*(2), 219–225.

Marshall, J., Adcroft, A., Hill, C., Perelman, L., & Heisey, C. (1997). A finite-volume, incompressible Navier Stokes model for studies of the ocean on parallel computers. *Journal of Geophysical Research*, *102*(C3), 5753–5766.

Marshall, J., Hill, C., Perelman, L., & Adcroft, A. (1997). Hydrostatic, quasi-hydrostatic, and nonhydrostatic ocean modeling. , *102*(C3), 5733-5752.

Martin, A. (2003). Phytoplankton patchiness: The role of lateral stirring and mixing. *Progress in Oceanography*, *57*(2), 125-174. doi: https://doi.org/10.1016/S0079-6611(03)00085-5

McGillicuddy, D., Robinson, A., Siegel, D., Jannasch, H., Johnson, R., Dickey, T., ... Knap, A. (1998). Influence of mesoscale eddies on new production in the Sargasso Sea. *Nature*, *394*(6690), 263–266.

Meeder, E. (2012). *Dynamics of nitrogen species in the oceanic water column* (Unpublished doctoral dissertation). The Hebrew University of Jerusalem.

Oschlies, A. (2002). Nutrient supply to the surface waters of the North Atlantic: A model study. *Journal of Geophysical Research: Oceans*, *107*(C5), 14-1-14-13. doi: https://doi.org/10.1029/2000JC000275

Paldor, N., & Anati, D. A. (1979). Seasonal variations of temperature and salinity in the Gulf of Elat (Aqaba). *Deep Sea Research Part A. Oceanographic Research Papers*, *26*(6), 661 - 672. doi: https://doi.org/10.1016/0198-0149(79)90039-6

Plähn, O., Baschek, B., Badewien, T., Walter, M., & Rhein, M. (2002). Importance of the Gulf of Aqaba for the formation of bottom water in the Red Sea. *Jour-*

nal of Geophysical Research, *107*(C8), 22–1.

Platt, T. C., Bird, D. F., Sathyendranath, S., & Cushing, D. H. (1991). Critical depth and marine primary production. *Proceedings of the Royal Society of London. Series B: Biological Sciences*, *246*(1317), 205-217. doi: 10.1098/rspb.1991.0146

Rasheed, M., Badran, M. I., Richter, C., & Huettel, M. (2002). Effect of reef framework and bottom sediment on nutrient enrichment in a coral reef of the Gulf of Aqaba, Red Sea. *Marine Ecology Progress Series*, *239*, 277–285.

Reiss, Z., & Hottinger, L. (1984). *The Gulf of Aqaba: Ecological micropaleontology* (Vol. 384). Springer-Verlag Berlin.

Rückelt, J. (2010). Optimization of parameters and initial values in a marine NPZD-type ecosystem model.

Salonen, K., Sarvala, J., Hakala, I., & Viljanen, M.-L. (1976). The relation of energy and organic carbon in aquatic invertebrates 1. *Limnology and oceanography*, *21*(5), 724–730.

Schartau, M., & Oschlies, A. (2003). Simultaneous data-based optimization of a 1d-ecosystem model at three locations in the North Atlantic: Part I—Method and parameter estimates. *Journal of Marine Research*, *61*(6), 765–793.

Silverman, J., & Gildor, H. (2008). The residence time of an active versus a passive tracer in the Gulf of Aqaba: A box model approach. *Journal of Marine Systems*, *71*(1), 159–170.

Smagorinsky, J. (1963). General circulation experiments with the primitive equations: I. The basic experiment. , *91*, 99-164.

Smetacek, V., & Passow, U. (1990). Spring bloom initiation and Sverdrup's critical-depth model. *Limnology and Oceanography*, *35*(1), 228–234.

Stambler, N. (2005). Bio-optical properties of the Northern Red Sea and the Gulf of Eilat (Aqaba) during winter 1999. *Journal of Sea Research*, *54*(3), 186–203.

Stambler, N. (2006). Light and picophytoplankton in the Gulf of Eilat (Aqaba). *Journal of Geophysical Research*, *111*(C11), 10.1029/2005JC003373.

Suggett, D. J., Stambler, N., Prasil, O., Kolber, Z., Quigg, A., Vazquez-Dominguez, E., ... Berman-Frank, I. (2009). Nitrogen and phosphorus limitation of oceanic microbial growth during spring in the Gulf of Aqaba. *Aquatic microbial ecology*, *56*(2-3), 227–239.

Sverdrup, H. U. (1953). On conditions for the vernal blooming of phytoplankton. *Journal du Conseil*, *18*(3), 287–295.

Wolf-Vecht, A., Paldor, N., & Brenner, S. (1992). Hydrographic indications of advection/convection effects in the Gulf of Elat. *Deep Sea Research*, *39*(7), 1393–1401.

Zarubin, M., Lindemann, Y., & Genin, A. (2017). The dispersion-confinement mechanism: Phytoplankton dynamics and the spring bloom in a deeply-mixing subtropical sea. *Progress in oceanography*, *155*, 13–27.